A reusable perfusion supporting tissue-mimicking material for ultrasound hyperthermia phantoms

Ronny B. Chin,[a] Ernest L. Madsen, James A. Zagzebski,[b] Hossein Jadvar, Xue-Kui Wu, and Gary R. Frank
Department of Medical Physics, 1530 Medical Sciences Center, University of Wisconsin, Madison, Wisconsin 53706

(Received 18 December 1989; accepted for publication 13 February 1990)

A new ultrasonically and thermodynamically tissue-mimicking material is reported. The material is well suited for use in phantoms for testing ultrasound hyperthermia systems or related predictive models. Controlled convective heat transfer effects, mimicking to some extent perfusive heat transfer in tissues, can be instituted in the material with appropriate fluid sources and sinks. The material consists of closely packed agar spheres varying in diameters from 0.3–3.6 mm. The interstitial space between spheres is filled with 10% *n*-propanol solution. The material has two practical advantages over the solid-gel-type tissue-mimicking materials. The first advantage is that it allows rapid return of a hyperthermia phantom to thermal equilibrium following a heating test by rapid circulation of the perfusion fluid. The second advantage is that the material is in a "liquid" form. It can be easily siphoned in and out of phantom containers of any geometric shape for different purposes without change in its physical properties. Methods for measuring ultrasonic and thermodynamic properties of the material and the results of the measurements are reported. The physical parameters measured are the intensity attenuation and absorption coefficients, the ultrasonic speed, the thermal conductivity, specific-heat capacity and the mass density. Temperature measurements in a hyperthermia phantom made of the material are also reported.

Key words: ultrasound phantom, thermal conductivity, convective cooling, perfusion, ultrasound hyperthermia

I. INTRODUCTION

One means for inducing local hyperthermia cancer treatment is based on absorption of ultrasound power in the region of a tumor. Various ultrasound hyperthermia systems are under development[1–7] or are already available commercially (Clini-Therm Corporation, Dallas, TX and Labthermics Technologies, Incorporated, Champaign, IL). Optimal systems, however, particularly regarding confinement of the significantly heated volume to the immediate region of a deep-lying tumor, have likely not yet been built.

In order to develop more effective deep-heating local ultrasound hyperthermia systems, one alternative is to construct systems based on intuitive qualitative understanding and test such systems on animals or on phantoms, simulating patients. This is a costly and time-consuming process. A better alternative is to develop accurate theoretical models for ultrasonic sources for predicting intensity distributions in tissue-like material and couple these with the bioheat equation[8] for predicting temperatures as a function of time and position. Then the deep heating properties of various ultrasonic sources could be tested via computer modelling until an optimal configuration has been deduced. Then, a real system, based on the computer optimization, could be assembled. Finally, the real system should be tested in realistic phantoms verifying that the desired heating patterns could be attained.

Phantoms used for testing ultrasound hyperthermia systems thus far reported, mimic tissues in terms of ultrasonic speed and attenuation/absorption properties.[9–11] However, these phantoms have not been shown to have the capacity for generating convective cooling similar to that due to blood perfusion in tissues. Thus the adequacy of theoretical models for accounting for the very important convective cooling has never been quantitatively tested.

If a phantom material is to mimic tissues quantitatively, then the thermal properties of the material must be accurately known and be tissue like. Also, some type of convective cooling must be producible which is representative of that in tissue. In this paper a perfusion supporting tissue-mimicking (PTM) material is described. The material allows a form of convection, which, while admittedly not accurately mimicking tissue perfusion in terms of zero local velocity, nevertheless provides a well-defined means for convective cooling. This report includes the following parts: (i) the composition and method of manufacture of the perfusion supporting tissue-mimicking material; (ii) the methods for measuring the ultrasonic and thermodynamic properties of the PTM material; (iii) a tabulation of ultrasonic and thermodynamic properties of the PTM material; (iv) the perfusion capability of the PTM material; and (v) measurements of time-dependent temperature distribution during ultrasound heating in a hyperthermia phantom made of the PTM material.

II. COMPOSITION OF THE PERFUSION SUPPORTING TISSUE-MIMICKING MATERIAL

The PTM material consists of closely packed agar spheres varying in diameter from 0.3–3.6 mm, the interstices being

 0094-2405/90/030380-11$01.20

filled with a solution of 10% *n*-propanol and 90% water (referred to as the propanol solution, hereafter). Histograms of the diameter distribution of the sphere are given in Fig. 1. The ordinate in Fig. 1(a) corresponds to the number fraction of spheres and in Fig. 1(b) corresponds to the volume fraction. In both figures the abscissa corresponds to diameter intervals. The spheres can be sufficiently close packed during filling of a phantom container that the solid part of the TM material (the spheres) forms a rigid mass, and the proponal solution is free to flow through the material in response to pressure gradients.

On the basis of density determinations of the 10% *n*-propanol solution, of the material composing the spheres, and of the composite PTM material, it is estimated that about $75 \pm 7\%$ of the volume of the PTM material consists of these agar spheres, the remaining volume being filled with the propanol solution.

The agar spheres themselves contain 3% dry-weight agar and 8.7% dry-weight talcum powder (type 8476, Mallinckrodt, Incorporated, St. Louis, MO), the remaining 88.3% consisting of one–part *n*-propanol and nine parts distilled water by volume (0.8–part *n*-propanol and nine parts water, by weight). The talcum powder consists of microscopic particles of talc and is uniformly distributed in each agar sphere. The presence of the talc particles is responsible for nearly all of the absorption of ultrasonic energy in the agar spheres, i.e., the loss of ultrasonic energy to heat.[12] The *n*-propanol serves to raise the ultrasonic speed to the range found in soft tissue and also to prevent bacterial invasion.

When the material is introduced into a phantom container, gravitational action together with tapping of the container causes the spheres to settle into a fixed relatively rigid configuration. This settling occurs because of the density difference between the spheres (1.05 g/cm^3) and the propanol solution (0.99 g/cm^3). Additional spheres must be added during the settling process. When the material is in this form, it is referred to as being in the "compact state." (In the compact state, the relative position of each agar sphere with the rest of the agar spheres cannot be changed.) It is in this state the material should exist in phantoms. Physical properties of the material should also be measured in the compact state, of course.

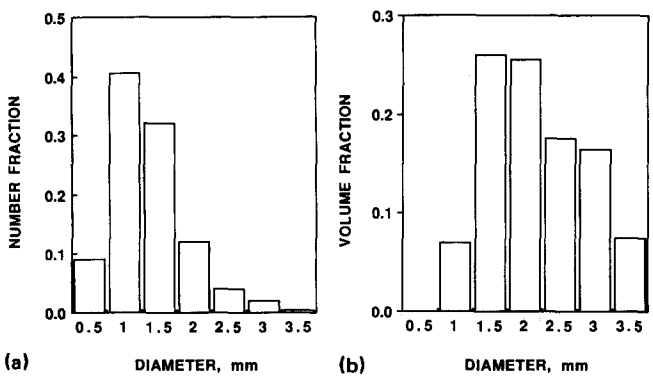

FIG. 1. Histograms of the diameter distribution of agar spheres in the PTM material. Plot (a) is the number fraction and plot (b) is the volume fraction of the spheres in terms of diameters.

III. METHOD OF PRODUCTION OF THE PTM MATERIAL

The agar spheres were mass-produced in our laboratory at the rate of about 2 l/h using the technique described below:

The basic idea involved is that of the "shot tower" used during the early days of the production of gun shot. In this case, the spheres formed are agar instead of lead, and the medium through which the congealing spheres fall is a kerosene–oil solution instead of air. The shot tower used is ~1 m high and the central column is filled with the kerosene–oil solution. A diagram is shown in Fig. 2. The upper section of the kerosene–oil solution is held at a temperature which exceeds the congealing temperature of the molten agar, and the lower section at a temperature of ~0 °C. These temperatures are maintained by one jacket, containing circulating hot water, surrounding the upper region and another jacket, containing ice water, surrounding the remaining lower part of the shot tower. Aluminum heat exchange tubes are also present.

During sphere production, molten agar, formed from 3% dry-weight agar and containing any desired particles in suspension, is ejected via hydrostatic pressure difference through small holes in rotating tubes; these tubes are part of a "shower head" appartus near the top of the tower. The shower head apparatus is depicted in Fig. 3. Upon ejection,

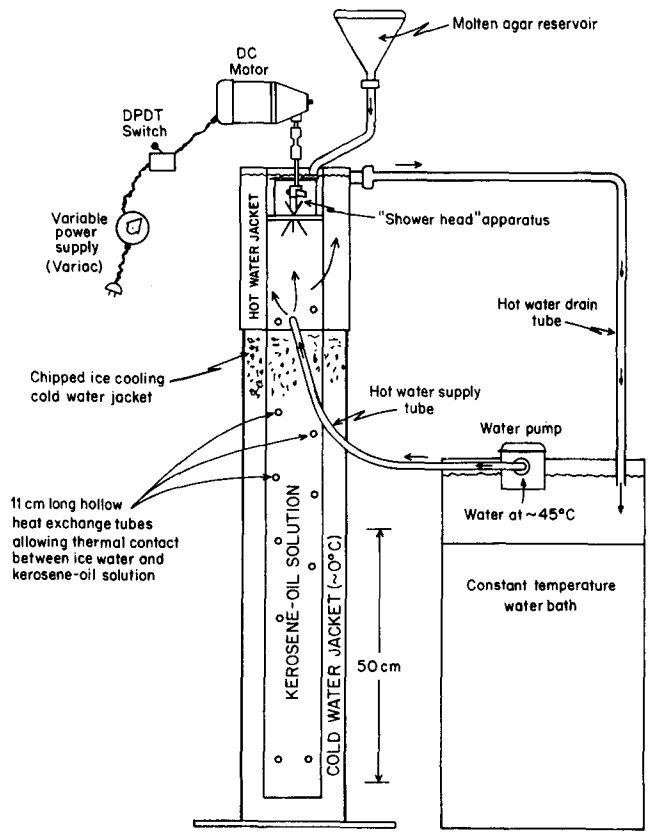

FIG. 2. Diagram of the shot tower assembly. The shot tower is filled with a mixture of kerosene and oil. The upper section is maintained at a temperature above the congealing temperature of the molten agar by a hot water jacket. The lower section is cooled by ice water to allow gradual congelation of the agar sphere.

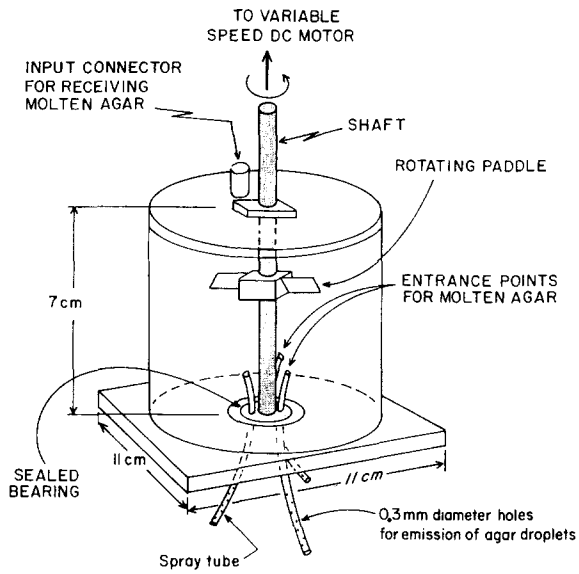

FIG. 3. Diagram of the "shower head" apparatus. The mixture of molten agar and talcum powder entering the shower-head housing is agitated continuously by the rotating paddle before being ejected from the spray tubes to ensure its homogeneity. The size of the ejected agar droplets is controlled by a variable-speed dc motor which rotates the spray tubes.

the molten agar forms into droplets, the mean diameter of which depends on the rate of rotation of the shower head. Thus, the mean diameter is controlled by the variable power supply driving the dc motor which rotates the ejection apparatus. Uniformity of the concentration of suspended talc particles inside the small droplets is assured through rotation of a paddle in the supply reservior from which the rotating tubes are supplied with molten agar. The agar droplets ejected into the hot kerosene–oil solution by the shower head immediately form into liquid spheres and descend through the less dense kerosene–oil. It takes only a few seconds for these liquid spheres to descend to the lower temperature region of the kerosene–oil column. Since the congealing temperature of the agar is 38 °C, the spheres likely congeal seconds after reaching the top of the lower temperature region. The distance from the shower head to the top of the lowered temperature kerosene–oil region is ~15 cm; thus, most of the 1-m length of the column consists of low-temperature kerosene–oil. The reason for the longer low-temperature region is that the apparatus can also be used to produce much larger spheres (up to ~6 mm in diameter) and these require a longer congealing time and, hence, a longer low-temperature section.

The congealed spheres are easily removed from the kerosene–oil solution by taking advantage of the fact that they are not only more dense than the kerosene–oil solution, but also more dense than water. Thus the kerosene–oil solution can be "floated" away from the spheres by addition of water. Spheres with diameters > 3.6 mm are then removed by sieving. For the specific material reported in this paper the removed spheres constituted ~5% by volume.

To produce diffusion equilibrium of the spheres with 10% *n*-propanol solution, the following procedure was employed. The water in the interstices was removed using a fine mesh sieve and the spheres introduced into an aqueous 10% *n*-propanol solution having a volume of at least three times that of the spheres. The combination was stirred occasionally throughout the day to aid the reaching of diffusion equilibrium. (The density of the spheres is ~6% greater than that of the solution; thus, the spheres always rapidly settle out.) The following day the above process was repeated, this time the residual *n*-propanol solution being removed first. Subsequently, the spheres are stored in an aqueous solution of 10% *n*-propanol.

IV. MEASUREMENT OF ULTRASONIC PROPERTIES

The ultransonic speed and attenuation coefficients were measured using through transmission techniques described in detail elsewhere.[13] The material is introduced in the compact form into test cylinders having inner dimensions of a 7.6-cm diameter and either a 2.5- or 5.0-cm length. The ultrasonic speed was measured at 1.0 MHz and the (amplitude) attenuation coefficient over a range of frequencies from 0.6–2.5 MHz.

The intensity attenuation coefficient α is the sum of two parts: an absorption coefficient α_a, corresponding to loss of ultrasonic energy to heat, and a scattering coefficient α_s corresponding to redirection of the (longitudinal) ultrasonic waves. An estimate of the absorption coefficient at 0.525 MHz was made in an experiment in which a focused ultrasound source was driven to produce a known continuous ultrasonic power P_o, the power being directed into a test cylinder filled with the PTM material. This experiment is, in essence, similar to that of Fry and Fry[14] in which absolute ultrasound intensity was used rather than the absolute power.

Consider a planar surface S that is perpendicular to the beam axis in the focal region of the transducer. The ultrasonic power P_D passing through S is closely approximated by the relation $P_D = P_o e^{-\alpha D}$, where D is the distance from the surface of the test cylinder (facing the transducer) to S as measured along the axis of symmetry of the transducer. P_o was kept low enough that nonlinear propagation should not have been significant.[15] (Also, below is given direct experimental evidence that nonlinear propagation effects were insignificant.) P_D must equal the integral of the intensity over the surface S. The intensity I of the beam at any point in the phantom can be expressed, as in Fry and Fry,[14] as

$$I = \frac{\rho c}{\alpha_a}\left(\frac{\partial T}{\partial t}\right)\Big|_o, \tag{1}$$

where ρ and c are the density and specific heat capacity, respectively, of the PTM material, and $(\partial T/\partial t)|_o$ is the initial rate of rise of temperature T as a function of time t immediately following the onset of ultrasound power. A copper–constantan thermocouple junction lying in the surface S, together with lateral translations of the transducer, allowed determination of a set of values of $(\partial T/\partial t)|_o$ so that the intensity over the surface S could be expressed through Eq. (1), all quantities being known except for α_a. The absorption coefficient α_a was determined by employing the relation

$$P_D = P_o e^{-\alpha D} = \int_S I ds = \frac{\rho c}{\alpha_a} \int_S \left(\frac{\partial T}{\partial t}\right)\Big|_0 ds. \quad (2)$$

That is,

$$\alpha_a = \frac{\rho c}{P_o e^{-\alpha D}} \int_S \left(\frac{\partial T}{\partial t}\right)\Big|_0 ds. \quad (3)$$

P_o was determined using a radiation force method.[16] A 1-cm-thick, flat absorbing target (Wallgone, Consumer Usage Laboratories, Rockville, MD) was placed in shallow container of degassed water, which was positioned on the stage of a digital balance (PM460, Mettler). The 0.525-MHz transducer was supported firmly above the balance with its radiating surface in the water and its beam axis perpendicular to the absorbing target surface. The digital balance measured the force on the target during brief intervals (3–5 s) of applied acoustic power. Since the target intercepted the entire beam, the total power is given by

$$P_o = uF, \quad (4)$$

where u is the ultasonic speed and F the force indicated by the balance. For an ultrasonic speed of 1490 m/s and if the balance reading is in grams, the applicable conversion factor is 14.6 W/g.

The temperature at the copper–constantan thermocouple junction was determined by monitoring the thermocouple voltage using a Hewlett–Packard 3497A data acquisition system, interfaced to a personal computer (IBM model AT) through an IEEE 488 General Purpose Interface Bus (National Instruments). The rate of temperature rise at the onset of power was found from a least-squares linear fit of the temperature versus time data for short (10–20 s) heating intervals.

The continuous-wave emitted power P_o used in the determined was 3.9 W. To corroborate experimentally that nonlinear propagation does not play a role, the emitted power was increased to 5.3 W and the value of $(\partial T/\partial t)|_o$ determined for the thermocouple at 9.0-cm depth and on the beam axis. Proportionality of emitted power and $(\partial T/\partial t)|_o$ was found, as expected, if propagation was linear.

V. MEASUREMENT OF THERMODYNAMIC PROPERTIES

A. Thermal conductivity

Accurate measurement of thermal conductivity was done using a basic concept given in many textbooks on thermodynamics. (See, e.g., Ref. 17) The material to have its thermal conductivity measured is made to fill the region between two concentric cylinders, the latter having thermal conductivities much higher than the interrogated materials. Heat can pass from one cylinder to the other only through the interrogated material, and the direction of heat flow is radial. Heat is deposited at a constant rate $\dot{Q}$ inside the inner cylinder and the outer cylinder is maintained at some constant temperature T_o. Also, $\dot{Q}$ is uniformly distributed along the length L of the inner cylinder which means that the temperature T_i' of the inner cylinder will be the same at all points, at any instant of time. The longer $\dot{Q}$ is applied, the closer T_i' will become to a (constant) asymptotic value T_i. Thus when the heat source has been on for a sufficiently long time, $T_i' \approx T_i$. Then, the thermal conductivity, κ of the interrogated material is given by

$$\kappa = \frac{\dot{Q}}{2\pi L(T_i - T_o)} \ln\left(\frac{D_o}{D_i}\right), \quad (5)$$

where D_o is the diameter of the outer cylinder at temperature T_o and D_i is the diameter of the inner cylinder at temperature T_i.

An apparatus for implementing the above method for measuring thermal conductivity was designed and constructed in our laboratory. The major mechanical components are depicted in Figs. 4 and 5. In Fig. 4 is shown the overall arrangement. Coaxial stainless-steel cylinders are arranged horizontally in a water bath maintained at a constant temperature T_o. At the ends of the stainless-steel cylinders, 2.5-cm-thick disks of very low thermal conductivity cellular ebonite insure that essentially the only paths for heat flow between the cylinders are in the interrogated material between them. The inner stainless-steel cylinder is filled with water plus a little alcohol ($\sim 5\%$) to prevent bacterial invasion. Also included inside the inner cylinder, are six straight lengths of 0.8-mm-diam nichrome heating wire parallel to the axes of the cylinders and connected (electrically) in series. Two thermocouple junctions are bonded with epoxy glue to the inside of the inner stainless-steel cylinder at positions shown in Fig. 5. Both thermocouples were monitored during measurements so that any (undesirable) nonuniformity in T_i over the length of the inner cylinder might be detected.

The nichrome heating wires are soldered to 0.9-mm-diam copper wires at one end of the inner cylinder. These copper wires pass through the cellular ebonite and are soldered to flexible braided 1.25-mm-diam insulated copper cables. The copper wiring has a very low electrical resistance compared to that of the nichrome.

In initial attempts to measure thermal conductivities, it was found that gravitationally induced convection currents in the solution filling the inner cylinder caused the temperature of the upper part of the inner cylinder to be unacceptably higher than that of the lower part. To eliminate this temperature nonuniformity, the coaxial cylinders are rotated at 6 rpm about their common axis using the dc motor shown in Fig. 4. Two radial 0.8-mm-thick acrylic constraints are epoxied to the inner surface of the outer stainless-steel cylinder (not shown in Fig. 5). These constraints extend the length of the cylinder and are ~ 2 cm in radial extent. Thus rotation does not enhance thermal exchange because the spheres remain fixed in position relative to the rotating apparatus. An electronic switch was included which reverses the direction of current flow in the dc motor after every 360° rotation to avoid damage to the wire leads.

During the measurement process, dc current I is provided to the nichrome wires at a constant voltage V by a Sorenson SRL 40-12 dc power supply (Sorenson Power Supplies, Manchester, NH), and V and I are monitored, respectively, with a Kiethley 130A and an HP 3466A digital multimeters. Since the copper wire has a negligible electrical resistance compared to that of the nichrome heating element,

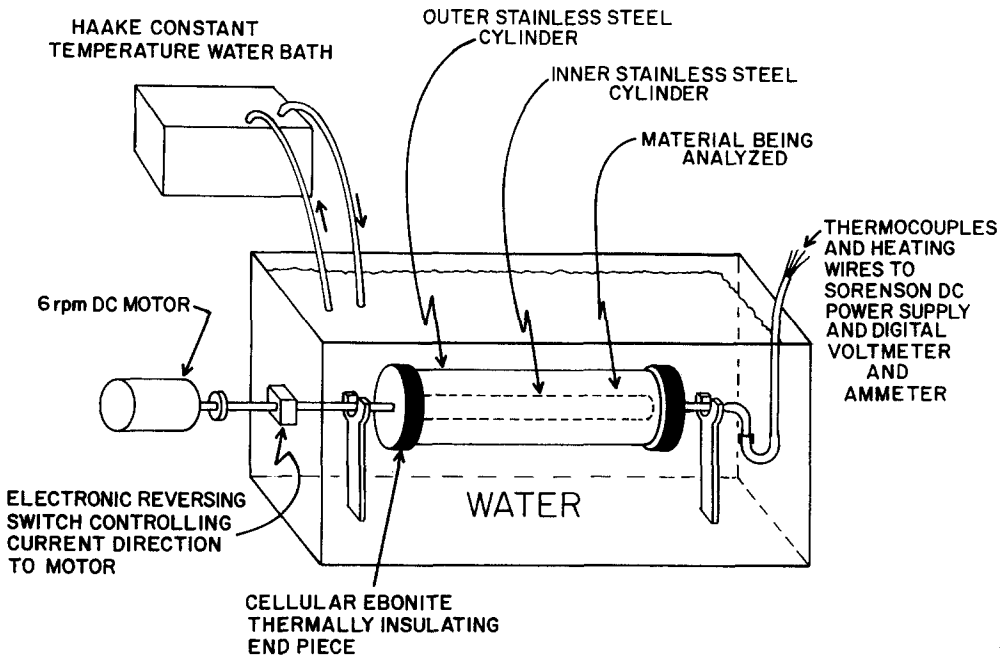

FIG. 4. Overall view of the components of the apparatus used for measuring the thermal conductivity of tissue-mimicking material. The cylindrical apparatus is rotated around a horizontal axis, back and forth, in alternating 360° cycles to reduce errors caused by gravitationally induced temperature gradients.

$\dot{Q} = I^2R \cong IV$ where R is the resistance of the nichrome wire. Thus Eq. (5) for the thermal conductivity can be written as

$$\kappa = \frac{IV}{2\pi L(T_i - T_o)} \ln\left(\frac{D_o}{D_i}\right). \tag{6}$$

The outer diameter of the inner stainless-steel cylinder (D_i) is 2.54 cm, the inner diameter of the outer stainless-steel cylinder (D_o) is 9.84 cm, and the length (L) is 36.8 cm.

In our measurements, the applied electrical power was such that the steady-state temperature difference was ~5 °C. The water bath temperature was monitored with an NBS calibrated thermometer accurate to within 0.01 °C. This thermometer was used to establish the accuracy of (and to calibrate) the thermocouple reader (model TH-8, Bailey Instruments, Saddle Brook, NJ).

The temperature at which the thermal conductivity was measured was taken to be the volume-averaged temperature. At steady state ($T_i' = T_i$) the temperature, $T(r)$, of the interrogated material at a distance r from the axis of symmetry of the system is given by

$$T(r) = T_i - \frac{T_i - T_o}{\ln(r_o/r_i)} \ln\left(\frac{r}{r_i}\right). \tag{7}$$

For $T_i = 25$ °C and $T_o = 20$ °C, the volume-averaged temperature of the interrogated material then is 21.6 °C ≈ 22 °C, a good approximation to room temperature, and we take

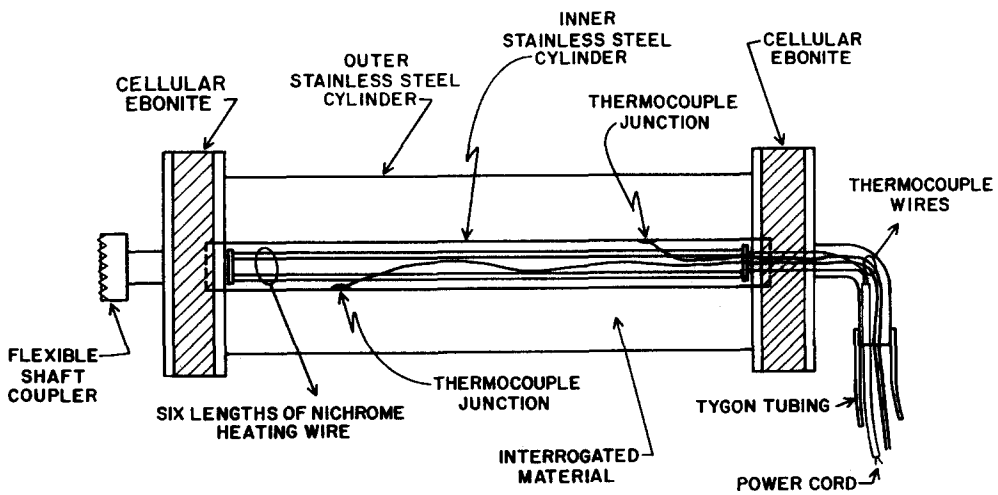

FIG. 5. Longitudinal cross-section of the apparatus used in the absolute measurements of thermal conductivities. Arrangement of the heating element, thermocouple wires, and the cellular ebonite thermal insulators is shown.

22 °C to be the temperature at which the thermal conductivity was determined.

The reproducibility (precision) of measurements of κ is $\pm$ 2%. The accuracy was tested by measuring the thermal conductivity of three different concentrations of agar gels which were poured into the measurement cavity of the apparatus and allowed to congeal. The concentrations were (1.5%, 3.0%, and 4.5% dry-weight agar Dico-Bacto agar, Difco Laboratories, Detroit, MI) dissolved in distilled water. In Table I are shown thermal conductivities determined with our apparatus for the three concentrations of agar, where T_o was about 20 °C and T_i about 25 °C. Also shown is the thermal conductivity for pure water at 22 °C.[17] The thermal conductivities are all within 2% of one another, and there appears to be no dependence on agar concentration. Therefore, the agar values are essentially that of pure water, the agar gel matrix serving only to suppress significant convection currents during measurements. These results indicate that the accuracy of our measured values approximate the precision, viz, $\pm$ 2%.

B. Specific heat capacity

A known mass of the PTM material maintained at a known temperature was placed inside a Dewar flask and covered by a cork. On the cork there are two holes which allow the insertion of a thermocouple and a catheter into the flask. The catheter was connected to a syringe externally. When the contents in the flask had reached thermal equilibrium, a known volume ($\sim$ 10% of the mass of the TM material) of 10% *n*-propanol solution at room temperature was injected into the flask by the syringe. Both the initial and final temperatures in the flask were recorded. When a new thermal equilibrium had been established in the flask, another volume of the 10% *n*-propanol at room temperature was added. The process was repeated for as long as was practical. The total mass of the PTM material and the propanol solution was determined by a Mettler PM460 digital balance after each addition of the propanol solution.

To simplify the analysis, let the initial temperature in the flask be T_o. Because of thermal insulation, no heat enters or leaves the Dewar container; therefore

$$c_g m_g (T_o - T) = c_a m (T - T_r), \tag{8}$$

where c_g and c_a are the specific heat capacities of the PTM material and the propanol solution respectively, m_g is the mass of the PTM material, m is the subsequently accumulated mass of propanol solution, T is the temperature in the flask after the addition of m, and T_r is the room temperature. Rearranging Eq. (8) gives

$$c_a m \frac{(T_o - T_r)}{(T_o - T)} = c_a m + c_g m_g. \tag{9}$$

The specific heat capacity of the TM material was determined from the y intercept of the plot of the term on the left on Eq. (9) versus m.

A separate experiment was performed to examine the accuracy of the method. A know mass of a solid-like TM material with a suspension of powdered graphite and distilled water were used. The data recorded was plotted using a version of Eq. (9) as follows:

$$m \frac{(T_o - T_r)}{(T_o - T)} = m + \left(\frac{c_g}{c_a}\right) m_g. \tag{10}$$

A plot of $m(T_o - T_r)/(T_o - T)$ versus m is shown in Fig. 6. Using a least-squares fitting, the slope of the line was determined to be 0.99, very close to the expected value of 1.00 It is concluded that heat lost due to imperfect insulation of the Dewar flask is negligible. Notice that for small m's in Fig. 6, the data points do not lie on the straight line. The reason is that for small m's, the value of $(T_o - T)$ is very small, resulting in a large uncertainty. Therefore, the initial data points were not used in the least-squares fitting.

C. Mass density

Density has relevance both ultransonically and thermodynamically. The densities of the PTM material and of the aqueous 10% *n*-propanol solution were determined using a 250.0-ml calibrated flask and a Mettler PM460 digital balance.

The density of material composing the spheres was determined using about 220 g of the bulk material (using 10% *n*-

TABLE I. Thermal conductivities for three concentrations of agar gel measured at 22 °C. The uncertainty in each value is $\pm$ 2%. A value for pure water at 22 °C is also shown; the latter was obtained by interpolation from tables.[17] All values are in Watts/m °C.

	percent dry weight agar		
water	1.5	3.0	4.5
0.592	0.600	0.584	0.600

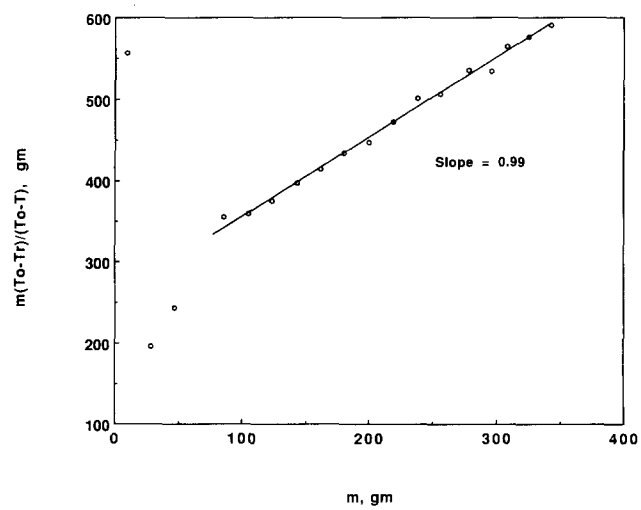

FIG. 6. A plot of Eq. (10) for determination of the accuracy of the specific heat measurement. Ideally the slope should be 1.00. The fluctuation of data points for small m is caused by the small difference between T_o and T.

propanol solution) which was formed in the usual manner in which solid tissue-mimicking material is manufactured in our laboratory.[18,19] First, about 90 ml of 10% *n*-propanol solution was introduced into a calibrated 250-ml graduate. A volume reading was obtained within ± 0.2 ml and the mass of graduate and solution, measured. Then the solid material was cut into pieces and introduced into the 10% *n*-propanol solution until the volume reading had been increased by ~ 150 ml. The final volume reading was then taken and the net mass of graduate, 10% *n*-propanol solution, and agar material, determined. The volume and mass of the agar material was then computed by taking the difference, the ratio equalling the density. The uncertainties in volume and mass determinations were estimated to be about $\pm 0.1\%$, and the net uncertainty in measured density is $\pm 0.2\%$.

D. Perfusion capability of the PTM material

The perfusion supporting tissue-mimicking material when packed in its compact state in a phantom container behaves like a porous medium in which fluid can be moved from one end to the other by pressure gradient. When perfusion of a fluid through a material can occur, the mean velocity, $\mathbf{v}$, of the perfusing fluid at a point $\mathbf{r}$ is proportional to ∇p, the pressure gradient. This is known as Darcy's law.[20] In mathematical form, Darcy's law can be expressed as

$$\mathbf{v} = \left(\frac{\lambda}{\eta}\right)\nabla p \tag{11}$$

where λ is the permeability of the material allowing perfusion and η is the viscosity of the perfusing fluid. The reciprocal of the ratio λ/η is of importance because it has the same dimensions as the volumetric blood perfusion rate used in the bioheat equation.[8]

The experimental set up as shown in Fig. 7 was used to measure the λ/η ratio. The PTM material was packed in its compact state and confined by stainless-steel screens in the central 40 cm region of a 60-cm-long right-circular cylindrical container. The inner cross-sectional area of the cylinder was 45.6 cm^2. At both ends of the cylinder were reserviors of 10% *n*-propanol solution which were connected to manometer tubes. During operation, clamp 1 is opened allowing siphoning of the *n*-propanol solution from beaker A into C, with concommitant overflow draining into beaker B, thus maintaining the hydrostatic pressure head in C, constant. Clamp 2 is also opened allowing fluid to leave reservior E and flow into beaker D. Thus, a steady-state flow is produced corresponding to the pressure difference $\Delta p = \rho g h$ where h is the difference in height of the fluid in the manometer tubes, ρ is the density of the *n*-propanol solution, and g is the acceleration due to gravity.

Measurement of h, the volume collected in beaker D per unit time, and the diameter and length L of the column of the PTM material allows computation of the λ/η ratio using Darcy's law. The average pressure gradient is given by $\rho g h/L$. The magnitude of the average velocity equals the volume of the fluid collected in beaker D per unit time, divided by the cross-sectional area of the column of the PTM material.

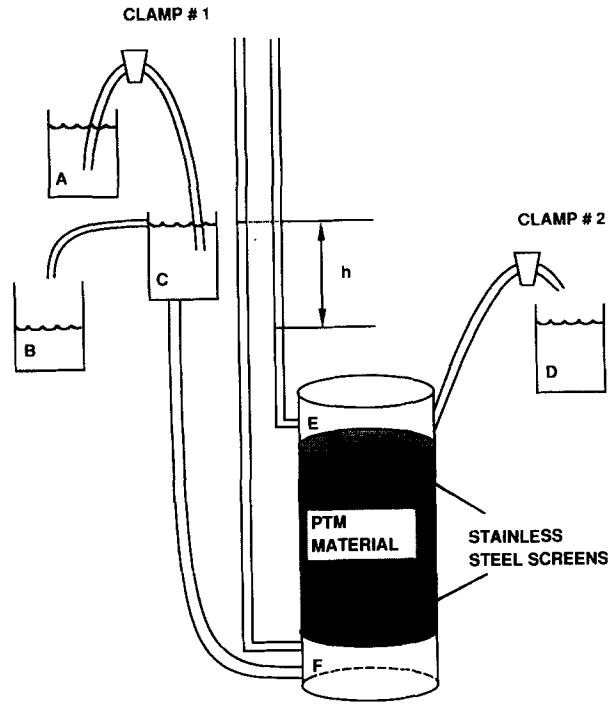

FIG. 7. Apparatus for measuring the λ/η ratio. The PTM material is packed in the shaded region between two stainless-steel screens in the cylinder. The propanol solution is siphoned from beaker (A) to beaker (C), the flow of which is controlled by clamp 1. The fluid enters the cylinder at reservior (F) and leaves at (E). Two manometer tubes are connected to reserviors (E) and (F) for measurements of pressure difference across the PTM material. Volume of the propanol solution perfused through the PTM material is collected per unit time in beaker (D).

VI. RESULTS

A. Ultrasonic properties

The ultrasonic speed of the PTM material is 1552 m/s and 1556 m/s at 22 and 27 °C, respectively; the uncertainty (specifying accuracy) is ± 2 m/s.[13] The attenuation coefficients were measured at three frequencies from 0.6–2.5 MHz and at 22 and 27 °C. Values given in dB/cm are tabulated in Table II. A linear relationship was observed between attenuation and frequency. The uncertainty (specifying accuracy, not just percision)[13] for each value is ± 0.05 dB/cm for measurements from 0.6–2.5 MHz.

In Table III are listed values for the absorption coefficient α_a and attenuation coefficient α correspond to 0.525 MHz and 1.06 MHz. The α at 0.525 MHz is computed from the measurements shown in Table II assuming a proprotionality of α and frequency between 0 and 1 MHz because the lowest

TABLE II. Attenuation coefficients of the PTM material at three frequencies in the range of those commonly used in ultrasound hyperthermia. The uncertainty in each value is ± 0.05 dB/cm.

Frequency (MHz)	22 °C α(dB/cm)	27 °C α(dB/cm)
0.60	0.55	0.55
1.00	0.85	0.84
2.50	1.89	1.96

TABLE III. Intensity absorption coefficient α_a and intensity attenuation coefficient α of the PTM material. The uncertainty in each value is $\pm$ 10%. The attenuation coefficient at 0.525 MHz is obtained by extrapolation from Table II.

Frequency (MHz)	α_a (cm^{-1})	α (cm^{-1})
0.525	0.086	0.116
1.060	0.147	0.196

frequency at which measurements of α can be made in our laboratory was 0.6 MHz.

The uncertainty in α_a was computed with the known uncertainties in ρ, c, α, D, P_o, and the $(\partial T/\partial t)|_o$'s. The finite nature of the area S in the integration may also contribute to the uncertainty. The dominant contribution to the uncertainty in α_a is that related to α. This leads to an estimate of the uncertainty in α_a of $\pm$ 10%.

B. Thermodynamic properties

In Table IV are shown values of thermal conductivity for the PTM material (designated "talc-type PTM material" in the table). Also shown, are values for two other types of tissue-mimicking materials as well as for a few types of soft tissue. The second tissue-mimicking material in the table consists of a solid block of agar in which the suspended particles giving rise to ultrasonic absorption consist of graphite instead talc. The concentration of graphite powder is 60 mg/ml. This concentration produced an attenuation coefficient of 0.70 dB/cm at 1.00 MHz which is considerably lower than the value of 0.85 dB/cm for the talc-type PTM material (Table II). The value of the thermal conductivity for a third type of material, ultrasonically fat tissue–mimicking material,[13] is also given. (Fat tissue-mimicking material consists of a dispersion of an olive-oil–kerosene mixture in a gel matrix; the material contains equal volume of oil and gel.[13]) At the bottom of Table IV are shown *in vitro* values of thermal conductivity for four types of soft tissues as measured by Bowman.[8] These are given for comparison with the values for the TM materials.

The specific heat capacity of the PTM material is determined to be 4.44 J/g °C at 27 °C (The specific heat capacity of 10% *n*-propanol is 4.27 J/g °C at 27 °C.[21]) The uncertainty estimated by least-squared fit is 0.13 J/g °C.

TABLE IV. Thermal conductivities at 22 °C for various ultrasonically tissue-mimicking and fat tissue-mimicking material, including the talc-based PTM material. Some *in vivo* tissue values, measured at 37 °C by Bowan,[8] are also shown for comparison purposes.

Material	Thermal conductivity (W/m °C)
Talc-type PTM material	0.555 $\pm$ 0.012
Solid agar containing graphite	0.635 $\pm$ 0.012
Fat tissue-mimicking material	0.300 $\pm$ 0.012
Kidney	0.547 $\pm$ 0.015
Skeletal muscle	0.508 $\pm$ 0.044
Liver	0.508 $\pm$ 0.028
Fat	0.222 $\pm$ 0.023

C. Mass density

The mass density is determined to be 1.036 g/cm^3. The limiting uncertainty in the density of the material composing the spheres is thought to come from the volume determinations. At best, the volume reading uncertainties were $\pm$ 0.2 ml. Because a volume difference was used, this translates into an uncertaintly of $\pm$ 0.3 ml, or about $\pm$ 0.2% of the 150 ml volume. Thus, the uncertainty in the density determination is taken to be $\pm$ 0.2%.

D. Perfusion capability

As shown in Fig. 8, at pressure gradients below 120 g/cm^2 s^2 a linear relationship between pressure gradient and average flow velocity was found in the range of 0.0 to 0.21 cm/s. The λ/η ratio determine from this linear relationship is 1.82×10^{-3} cm^3 s/g (or reciprocal of 551 g/cm^3 s). At pressure gradients above 120 g/cm^2 s^2, the λ/η ratio decreases monotonically, an indication of turbulent flow across the PTM material.

VII. TEMPERATURE MEASUREMENTS IN A PTM PHANTOM

One major application of the perfusion supporting tissue-mimicking material is in phantoms for testing ultrasound hyperthermia applicators or related predictive models. A phantom has been built with the PTM material for experimental verification of a thermal model. This thermal model accounts for the rate of energy change in a homogeneous and nonperfused tissue volume due to thermal conduction and absorption of ultrasonic energy. Results from this experiment are shown here in part to demonstrate the value of the PTM material as an ultrasound hyperthermia phantom material.

A focused ultrasound transducer with projected radius of 3.0 cm, radius of curvature of 9.4 cm, operating frequency of 0.525 MHz, and power of 3.9 W was used to insonify a phantom made of the PTM material. The change of temperature as a function of time at 6.5-, 9.0-, and 11.0-cm depths along the ultrasound beam axis in the phantom are compared to predictions of the thermal model. The results are plotted in Fig. 9 in which the solid lines represent thermal model predictions and the circles represent experimental measurements.

VIII. DISCUSSION

The attenuation coefficient values for the talc-type PTM material in Table II are in the range of those of soft tissues at corresponding frequencies. The same is true for the ultrasonic speed given in Table V. For comparison, see values for liver and muscle, e.g., in the compilation of data by Goss *et al.*[22] No significant dependence of attenuation coefficient on the temperature was observed over the 5 °C range from 22–27 °C. Thus, in using the phantom for quantitative tests of ultrasound hyperthermia systems the attenuation coefficient can reasonably be considered a constant.

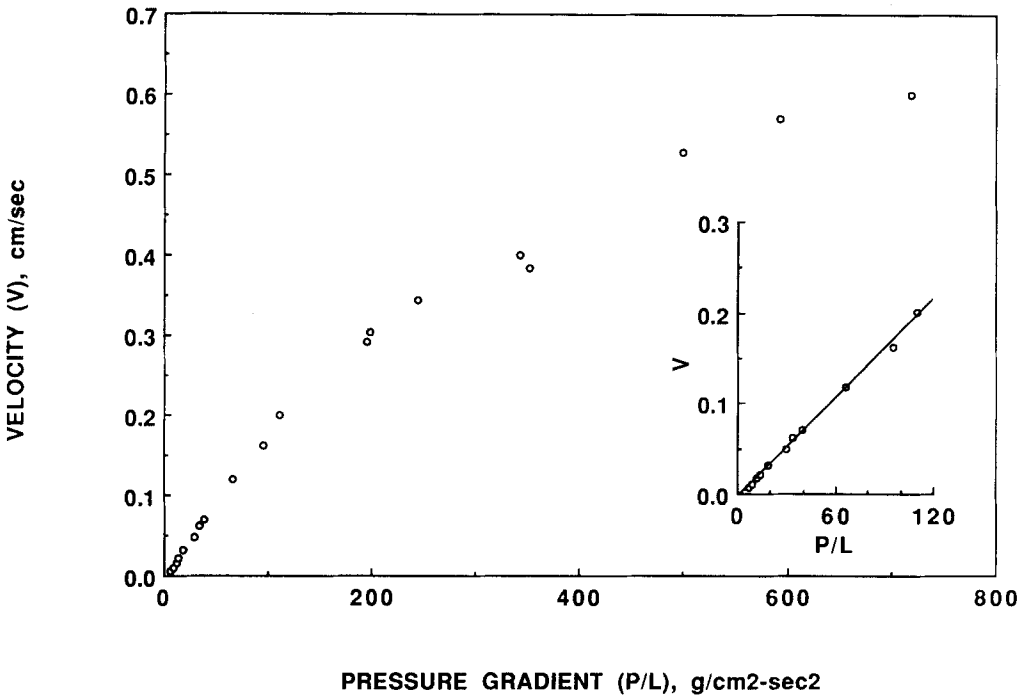

FIG. 8. Graph used in determination of the λ/η ratio. The mean velocity of the *n*-propanol solution flowing through the PTM material as a function of externally applied pressure gradient is shown. A linear relationship exists at low pressure gradients as shown in the inset, the slope of which is the λ/η ratio. At high pressure gradients, the curve deviates towards the abscissa, indicating the existence of turbulent flow.

The intensity absorption coefficient measured for this material at 0.525 and 1.06 MHz and 22 °C is 74% and 75% of the intensity attenuation coefficient, respectively. Thus, absorption dominates scattering in the attenuation, even at such low frequencies. Scattering of compressional waves at 0.525 MHz in the PTM material is likely due almost entirely to density fluctuations in the materials between that in the spheres (1.05 gm/cm^3) and that of the 10% *n*-propanol solution (0.99 gm/cm^3) in the gaps between the spheres. As mentioned above, the volume fraction consisting of the 10% *n*-propanol is about 0.25.

Following, is an argument that the absorption coefficient, like the attenuation coefficient, is relatively temperature independent. The density of pure water drops from 0.99820 gm/cm^3 to 0.99565 at 1 atm as the temperature increases from 20–30 °C.[23] Since the spheres and the solution are mostly water, there is probably also little density variation in these material over a 10 °C range. Thus, the fraction of the attenuation coefficient due to scattering should be relatively temperature independent. Since the attenuation coefficient is temperature independent and the absorption coefficient is the difference between the attenuation coefficient and the scattering coefficient, the absorption coefficient must be comparably independent of temperature.

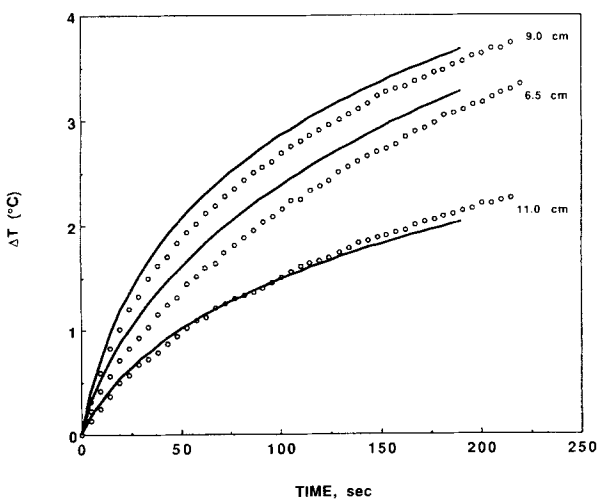

FIG. 9. Temperature changes, as a function of time, along the beam axis of a focused ultrasound transducer and at 6.5, 9.0, and 11.0-cm depths in the phantom. Thermal model predictions are represented by the solid lines and experimental measurements by the circles.

The values for thermal conductivity of some tissue types in Table IV indicate that this parameter ranges from about 0.50 to 0.55 W/cm^{-1} °C for nonfat tissue. The value of 0.555 W/cm^{-1} °C for the talc-based PTM material approximates this range rather well. However, the thermal conductivity of the graphite-containing material, commonly used in diagnostic ultrasound phantoms, is 14% higher than that of the talc-based PTM material, even though the attenuation coefficients of the two materials at 1.00 MHz are related in the inverse way. (The attenuation coefficient of the talc-based PTM material is 0.85 dB/cm at 1.00 MHz and is 0.70 dB/cm for the graphite-based material.) Thus for hyperthermia phantom materials, talcum powder appears to be superior to graphite powder for use in mimicking the ultrasonic absorption coefficient of tissues while at the same time mimicking the thermal conductivity of nonfat-type soft tissues.

Regarding ultrasonically fat tissue-mimicking material, the value of the thermal conductivity shown in Table IV is considerably less than that of the talc-based PTM material. The value is $\sim\frac{4}{3}$ that for *in vitro* real fat shown in the table. Thus the fat tissue-mimicking material is rather good regarding its ability to mimic the thermal conductivity of real fat.

The specific heat capacity of the PTM material is ~6%

higher than that of water, a fact which when combined with the fact that the density of the material is ~4% higher than that of water, means that the volumetric specific heat capacity ρc is ~10% higher than that of water.

The uncertainty for the thermal conductivity measurements is ± 2%, for the specific heat capacity, ± 3%, and for the density, ± 0.2%. For all three parameters, the rate of change with temperature is likely, similar to that for water since the material is mostly water. The change in these parameters with temperature for water is less than 1% over a 10 °C range about room temperature (22 °C).[23] Thus, the values in Table V should be acceptable as constants in a hyperthermia phantom in which temperature rises produced in quantitative tests of theoretical models are likely not more than 10 °C above the initial room temperature value.

To achieve uniformity and isotropy of the convection properties of the PTM material, it is required that the spatial distribution of spheres by size be random. This can be assured by introducing the material into a phantom via siphoning. To do this, the material in its pseudoliquid form is first mixed well so that the source container possesses randomness of spatial distribution. Rapid siphoning into the control region of the material in the receiving container accomplishes the desire result. Once the material has been transferred in the pseudoliquid state, the compact state can be brought about by tapping or vibrating the walls of the receiving container, more spheres being added as settling occurs.

Heat transport via convection can be instituted in the material in order to test heating systems in a way having some degree of similarity to heat transport via blood perfusion in tissues. This convection should be implemented when the material is in its "compact" state such that only the perfusion fluid can move through the material in response to externally applied pressure gradients. The convective heat transport producible in the material will not accurately simulate tissue perfusion in terms of zero local velocity. Nevertheless, convection velocity distributions can be well defined by appropriate choices of source and sink geometries and these velocity distributions can produce rates of exchange of "arterial" and "venous" blood similar to those found in blood perfusion.

IX. SUMMARY AND CONCLUSIONS

An ultrasonically and thermodynamically tissue-mimicking material has been described and the relevant properties given so that the material can be used in phantoms for quantitative testing of ultasound hyperthermia systems. The methods by which the properties were measured and by which errors were estimated have been thoroughly described.

The nature of the material provides two partical advantages not possible in the commonly used solid-gel ultrasonic TM materials.[18,19] A very useful practical quality of the material is that rapid flow of solution can be set up in the material with appropriate source and sink geometries and pressure gradients. By circulation of the perfusion fluid and passing it through an external temperature regulating device, uniformity of temperature in a phantom could be rapidly recovered following (localized) ultrasound heating. Thus much less time would be required to do successive heating tests on a phantom starting from a condition of uniform temperature than when a solid phantom material is used.

Another practical advantage of the material is that by temporarily introducing an excess of solution the material becomes slurry-like and can be poured or siphoned from one container to another. Following transfer it can be returned to its compact state. Thus, the material can be reused many times. This allows inner components of a phantom to be repaired or changed (such as thermocouples)—or entirely new phantoms to be produced—without the need for extensive cleanup procedures or for making and measuring the properties of additional tissue-mimicking materials.

TABLE V. The ultrasonic and thermodynamic properties of the PTM material at 22 °C. The attenuation and absorption coefficients were measured at 1 MHz.

Ultrasonic speed	1552 ± 2 m/s
Intensity attenuation coefficient	0.196 ± 0.020 cm^{-1}
Intensity absorption coefficient	0.147 ± 0.015 cm^{-1}
Thermal conductivity	0.555 ± 0.011 W/m °C
Specific heat capacity	4.44 ± 0.13 J/g °C
Mass density	1.036 ± 0.002 g/cm^3

ACKNOWLEDGMENTS

This work has been supported in part by National Institute of Health Grants R01 CA38865 and R01 CA25634. We thank Orlando Canto for providing some of the figures.

[a] Current address and reprint request: Department of Radiation Oncology, University of Rochester, 601 Elmwood Avenue, Box 647, Rochester, NY 14642.

[b] Also Departments of Human Oncology and Radiology.

[1] P. Corry, B. Barlogie, W. Spanos *et al.*, "Approaches to clinical applications of combinations of nonionizing and ionizing radiations," in *Radiation Biology in Cancer Research*, edited by R. Meyer and H. Withers (Raven, New York, 1980), pp. 637–644.

[2] J. Marmor, D. Pounds, T. Postic, and G. Hanh, "Treatment of superficial human neoplasma by local hyperthermia induced by ultrasound," Cancer **43**, 188–197 (1979).

[3] P. Fesenden, E. R. Lee, T. L. Anderson, J. W. Strohbehn, J. L. Meyer, and T. V. Samulski, "Experience with a multitransducer ultrasound system for localized hyperthermia of deep tissue," IEEE Trans. Biomed. Eng. **31**, 126–135 (1984).

[4] K. Hynynen, D. Watmough, and J. Mallard, "Local hyperthermia induced by focused and overlapping ultrasonic fields–and *in vivo* demonstration," Ultrasound Med. Biol. **9**, 621–627 (1982).

[5] P. Higgins, X. Zeng, and J. Zagzebski, "Versatility of distributed focus ultrasound in treatment of superficial lesions," Int. J. Rad. Onc. Biol. Phys. **10**, 1923–1931 (1984).

[6] R. Beard, R. Magin, L. Frizzell, and C. Cain, "An annular focus ultrasonic lens for local hyperthermia treatment of small tumors," Ultrasound Med. Biol. **8**, 177–184 (1982).

[7] P. Lele, "An annular focus ultrasonic lens for production of uniform hyperthermia in cancer therapy," Ultrasound Med. Biol. **7**, 191–192 (1981).

[8] H. F. Bowman, "Thermodynamics of tissue heating: modelling and measurements for temperature distributions," in *Physical Aspects of Hyperthermia*, edited by G. H. Nussbaum (American Institute of Physics, New York, 1982), pp. 511–548.

[9]K. Hynynen, D. J. Watmough, and J. R. Mallard, "The effect of thermal conduction during local hyperthermia induced by ultrasound: a phantom study," Br. J. Cancer (suppl.) **45**, 68–70 (1982).
[10]P. D. Edmunds, W. C. Ross, and P. Fessenden, "Spatial distributions of heating by ultrasound transducers in clinical use, indicated in a tissue-equivalent phantom," in *Ultrasonics Symposium Proceedings*, (Institute of Electrical and Electronics Engineering, New York, 1985), pp. 908–912.
[11]P. D. Higgins and F. Jafari, "Thermal distributions in spherical regions with variable thermal conductivity," IEEE Trans. Ultrasonics, Ferroelectrics, and Frequency Control **33**, 21–26 (1986).
[12]X. K. Wu, M. M. Goodsitt, and E. L. Madsen, (unpublished).
[13]E. L. Madsen, J. A. Zagzebski, and G. R. Frank, "Oil-in-gelation dispersions for use as ultrasonically tissue-mimicking materials," Ultrasound Med. Biol. **8**, 277–287 (1982).
[14]W. J. Fry and R. B. Fry, "Determination of absolute sound levels and acoustic absorption coefficient by thermocouple probes—experiment," J. Acoust. Soc. Am. **26**, 311–317 (1954).
[15]T. G. Muir and E. L. Carstensen, "Prediction of nonlinear acoustic effects at biological frequencies and intensities," Ultrasound Med. Biol. **6**, 345–357 (1980).
[16]S. A. Goss, R. L. Johnson, V. Maynard, L. Nider, L. A. Frizzell, W. D. O'Brien, Jr., and F. Dunn, "Elements of tissue characterization," in *Ultrasonic Tissue Characterization*, edited by M. Linzer (Spec. Publ. 525, U.S. Government Printing Office, Washington, D.C., 1979), Vol. II, pp. 43–51.
[17]M. W. Zemansky, *Heat and Thermodynamics*, 4th ed. (McGraw-Hill, New York, 1957), p. 82.
[18]E. L. Madsen, "Ultrasonically soft tissue-mimicking materials ans phantoms," in *Tissue Characterization with Ultrasound, Volume I: Methods*, edited by J. F. Greenleaf (CRC, Boca Raton, Florida, 1986), pp. 165–181.
[19]M. M. Burlew, E. L. Madsen, J. A. Zagzebski, R. A. Banjavic, and S. Sum, "A new ultrasound tissue equivalent material with a high melting point and extended speed of sound range," Radiology **134**, 517–520 (1980).
[20]F. A. L. Dullien and V. K. Batra, *Flow Through Porous Media* (Amer. Chemical Soc., Washington, D.C., 1970).
[21]*International Critical Tables*, Vol. 5, Edward W. Washburn (Editor-in-chief) C. J. West and N. E. Dorsey (Assoc. ed.) (McGraw-Hill, New York, 1929), p. 113.
[22]S. A. Goss, R. L. Johnson, and F. Dunn, "Comprehensive compilation of empirical ultrasonic properties of mammalian tissues," J. Acoust. Soc. Am. **64**, 423–457(1978).
[23]G. W. C. Kaye and T. H. Laby, *Tables of Physical and Chemical Constants*, 14th ed. (Longman, London, 1973), p. 61.